AT 39.3/116

ATCA Antenna Beam Patterns and Aperture Illumination

Jared Cole and Ravi Subrahmanyan
July 2002

Detailed here is a method and results from measurements of the beam characteristics of the ATCA antennas. We have used a celestial radio source, in the observing bands of the receivers, in preference to a satellite beacon signal. Scans over the source were made to derive the beam patterns, and these were Hankel transformed to derive the amplitude of the radial aperture illumination. The advantage of this is that the measurements are taken at normal operating frequencies, using a normal feed, giving results that are relevant to the telescope performance for astronomical observations. It may be noted here that holography at the ATCA has used a special feed that purposely over-illuminates the edges of the antenna.

Procedure

The conventional method for measuring radio telescope radiation patterns is to locate a suitable satellite beam signal and measure the strength of this signal in total power, with the pointing of the antenna offset to various positions. Using this method, its possible to determine the far field radiation pattern as a function of angle from the optical axis. Using the ATCA's multiple antennas, it is possible to perform a similar analysis using interferometry measurements of natural radio sources. This method relies on using one antenna as a "reference" antenna and pointing one or more of the other antennas at various offsets. The calibrated complex visibilities are a measurement of the far field voltage radiation pattern (of the antenna that is offset). Once this voltage radiation pattern has been determined, it can be used to calculate the complex aperture illumination distribution across the antenna.

In this investigation we did not wish to perform a full holographic analysis but only to measure the far field beam patterns through the optical axis of the antenna. As such, we have assumed the beam patterns as well as the aperture illuminations are axially symmetric and, therefore, they are both purely radial functions. The blockage due to the quadrupod structure is neglected.

To measure the far field pattern, two perpendicular scans were taken through the optical axis of the telescopes in the MOSAIC mode of operation. These scans were oriented at 45° to the quadrupod structure, to ensure that the effect of this structure on the measurements was minimised. Data were acquired for 10 sec integration times at each offset pointing; antenna slew typically took 3 sec and we obtained an effective time of 7 sec at each position. The scan directions and order for the offset positions are illustrated as Figure 1.
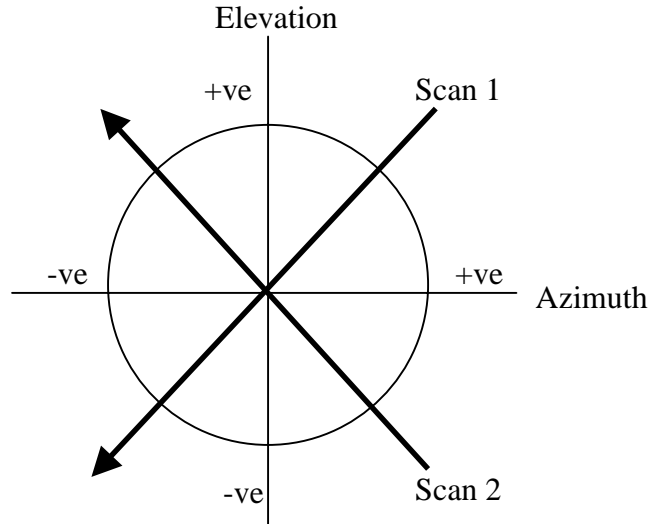
Figure 1 : Scan Directions and Orientation

In order to create a mosaic file, to provide the telescope with the offset angles for the measurements, the angular increment and maximum deflection needed to be calculated. As the beam pattern is related to the aperture distribution through the two-dimensional Fourier or Hankel Transform, we can use basic Fourier theory to derive these quantities. The angular increment required to avoid aliasing in the aperture domain can be related to the maximum radial extent of the aperture illumination; this is the radius of the main reflector. Additionally, the maximum offset from the bore-sight to which measurements are required to be made is related to the resolution with which we wish to sample the aperture distribution. These relations are shown below (1 & 2) where θ_{max} is the maximum deflection, $\Delta\theta$ is the step size required, λ is the wavelength of the radiation of interest, D is the diameter of the dish and δd is the required resolution of the aperture distribution.

$$\theta_{max} = \frac{\pm\lambda}{2\delta d} \qquad (1)$$

$$\Delta\theta = \frac{\lambda}{D} \qquad (2)$$

Equation 2 is the Nyquist sampling criterion. In practice, we over-sampled the beam by, at least, a factor of 2. Each of the two cross scans, at each frequency, was done twice: once with fine sampling and over a limited range of angular offsets from the source, second with a coarse sampling and over a wide range of angular offsets. It may be noted here that equation 1 assume that the data is not tapered (windowed); the application of a window to the scan data will reduce the resolution in the computation of the aperture distribution.

In order to provide accurate calibration of the complex visibilities and the resulting complex voltage pattern, the telescope must return to the target at regular intervals.

Several boresight observations were inserted during the beam scans and this data was used to calibrate out the time variations in the complex antenna gains. The dwell time for the boresight position and upon returning to the scan were increased, to account for the longer slews.

Once the observations had been taken, the results were calibrated for both amplitude and phase (using standard MIRIAD calibration procedures). In the case of continuum sources, a band-pass calibration was also performed prior to channel averaging. The resulting complex scan data were then exported as ASCII format files for further analysis. The raw data was then processed by a series of routines, written in C, to average, collect, compare and display the antenna field patterns.

To produce the aperture distribution as a function of distance from the centre of the antenna, a routine was written to perform a Hankel Transform, 3. The routine implemented a discrete version of this Transform; we have coded the expression in 4, where q is the angle in radians, Δq is the angular increment, F(q) is the far field voltage beam pattern that is measured at 2n+1 offset positions, r is the radial distance in wavelengths and f(r) is the aperture illumination (again a voltage and not power).

$$f(r) = 2\pi \int_0^\infty F(q) J_0(2\pi q r) q \, dq \tag{3}$$

$$f(r) \approx \pi F(0) \left(\frac{\Delta q}{2} \right)^2 + 2\pi \sum_{i=-n}^{+n} F(q_i) J_0(2\pi q_i r) q_i \Delta q \tag{4}$$

In order to improve the point spread function for the aperture distribution a windowing algorithm was also implemented. This function reduces the ringing due to sharp edges in the aperture amplitude distribution (due to the side-lobes of the point-spread function). The Hamming window function (5) was selected.

$$w(n) = 0.54 - 0.46 \cos(\frac{2\pi n}{N-1}), \ 0 \le n \le N-1 \tag{5}$$

Results and Analysis

Throughout this analysis it is assumed that the antennas are symmetrical about the optical axis; therefore the averaging and transforms were performed on data sets representing a scan from the centre to the maximum offset angle. Each complete scan was therefore broken into two sections, representing the scan towards and then away from the centre. These were then averaged to improve measurement sensitivity. Each beam pattern displayed is two sided; this has been achieved by artificially reflecting the data through the optical axis, purely to make the display more understandable.

This assumption, that the pattern is symmetrical, is not valid for the high frequency measurements (86 GHz). At these high frequencies, the asymmetric deformations in the main reflector and off-axis displacements in the sub-reflector, due to gravity, make the beam pattern asymmetric (although the aperture amplitude distribution ought to be symmetric). While the measurements showed asymmetric beams in the W band measurements, no detailed analysis of this aspect will be performed herein.

Antenna Field Patterns

Using the method detailed above, measurements were taken at frequencies in the C, X, K and W bands. In the C and X bands, two frequency channels were used, with a bandwidth of 128 MHz, while in the K and W bands only one frequency was used with a bandwidth of 64 MHz. The exact frequencies and astronomical sources used can be seen in Table 1, as well as the range of azimuth and elevation over which the sources were observed. For the C and X band measurements, continuum sources were used, while for K and W band maser lines were used. For all except the W band measurement, antenna CA02 was used as the reference. For the W band measurement, this was changed to antenna CA03 to avoid shadowing of the scanning antenna.

Band	Frequency (GHz)	Source Name	Azimuth Range (deg.)	Elevation Range (deg.)
C	4.800/4.928	2134+004 9.9 Jy continuum	320-370	52-58
X	8.512/8.640	1730-130 10.5 Jy continuum	283-312	46-60
K	22.2355	VX-Sgr H_2O maser line	72-88	50-69
W	86.2435	Orion SiO maser line	65-79	28-45

Table 1 : Frequencies and Sources

All the measurements shown here were taken with the array in the 1.5G configuration. The C and X band measurements were taken between 10pm and 4:30am on the evening of Wednesday the 3rd of July 2002. The K band measurements were taken between 8pm and 12am on the evening of the 4th of July and the W band measurements were taken between 6am and 9am the following morning (5th of July).

The continuum sources are strong enough so that with 7 sec integration, the noise on a single baseline, single polarization product, is about 0.0015 of the signal amplitude; this is good enough to measure the voltage pattern down to –28 dB or the power pattern down to –56 dB. The signal-to-noise on the maser sources, which were used for the beam pattern measurements at the higher frequencies, are better.

For each plot showing a comparison of beam patterns at different frequencies, the angle axis has been scaled to allow a comparison of the beam shapes. The actual maximum angular displacement and angular increment used for the course and fine scans are shown in Table 2. The ratio of the angular displacements in this table can be used to calculate the actual angular distribution.

Frequency (GHz)	Course Scans		Fine Scans	
	θ_{max} (deg)	$\Delta\theta$ (deg)	θ_{max} (deg)	$\Delta\theta$ (deg)
4.800/4.928	5.1040	0.0580	0.8400	0.0210
8.512/8.640	2.8160	0.0320	0.4720	0.0118
22.2355	1.0912	0.0124	0.1840	0.0046
86.2435	0.2816	0.0032	0.0480	0.0012

Table 2 : Angular Spacing and Range used for Scans

Based on the measurements, it was found that there is little variation in the far field patterns between different antennas in the array and between the different polarizations. The main lobe showed no noticeable variation and the side lobes only minor variations between the antennas. Based on this observation, the data has been averaged across all antennas, in order to improve the sensitivity in the measurements.

When scaled based on frequency, the antenna far-field patterns at the different frequencies show very little variation, as can be seen in Figure 2. It can be seen, however, that at the highest frequency (W-band), the side lobes are noticeably higher than in the lower frequency bands.
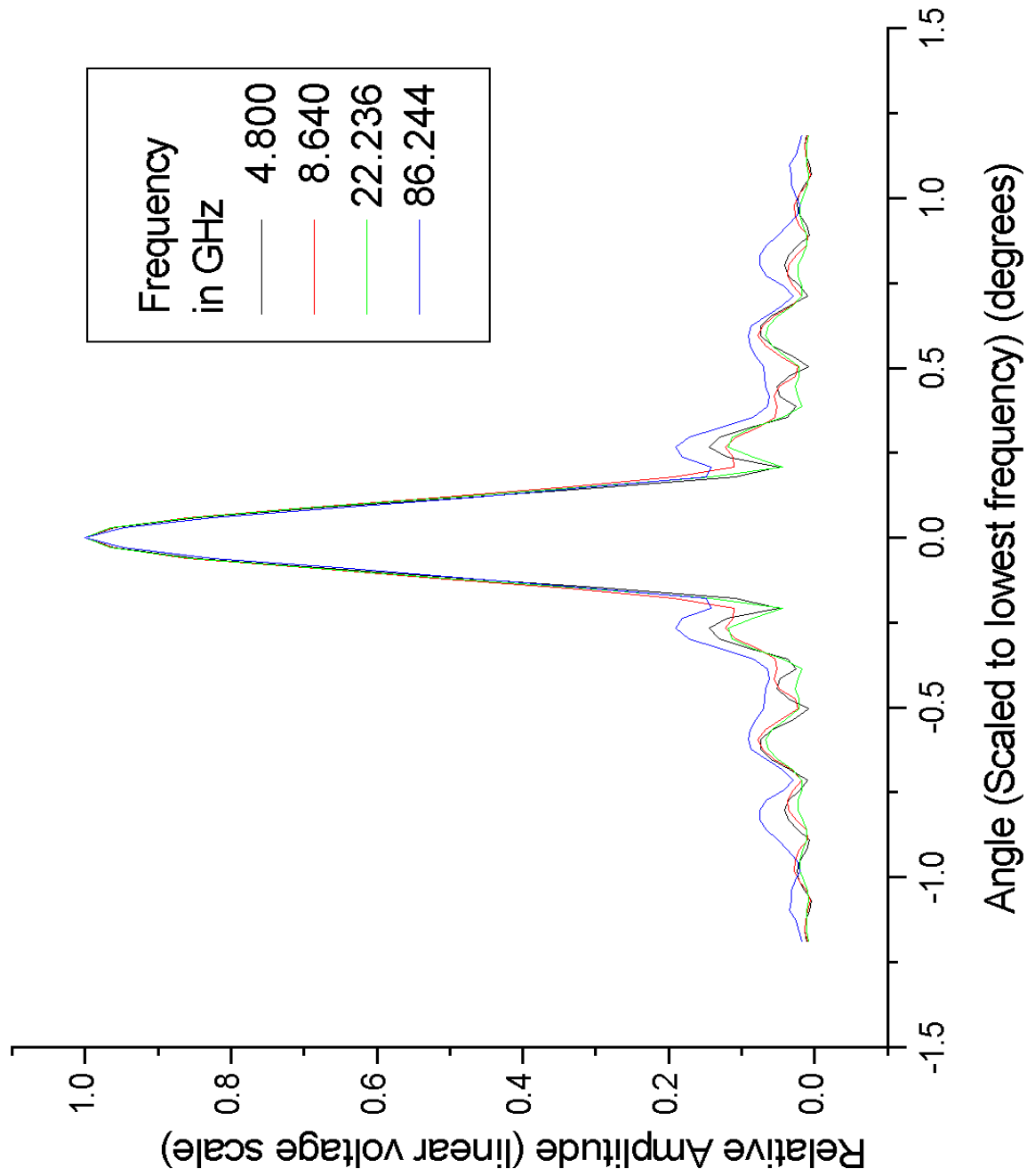
Figure 2 : Voltage radiation patterns in the C, X, K and W bands

Using the power pattern at each frequency, the FWHM was calculated. The results are given in Table 3 and show the "half-power beamwidth" at each frequency.

Band	Frequency (GHz)	Beam Width (arc mins)
C	4.800	10.171
C	4.928	10.022
X	8.512	5.957
X	8.640	5.909
K	22.2355	2.344
W	86.2435	0.544

Table 3 : Half Power Beam Widths

In order to examine the symmetry of the beam, the radiation pattern was plotted for two polarisation's, XX and YY, and for the two scan directions, as indicated in Figure 1. For a circular beam shape, these scans should all be coincident, this was found to be the case for the C, X and K band measurements. Shown in Figure 3 are the results for the C band measurements, which show a circular beam shape. The X and K band measurements proved to be very similar, indicating the beam shape is circular up to at least 22 GHz.
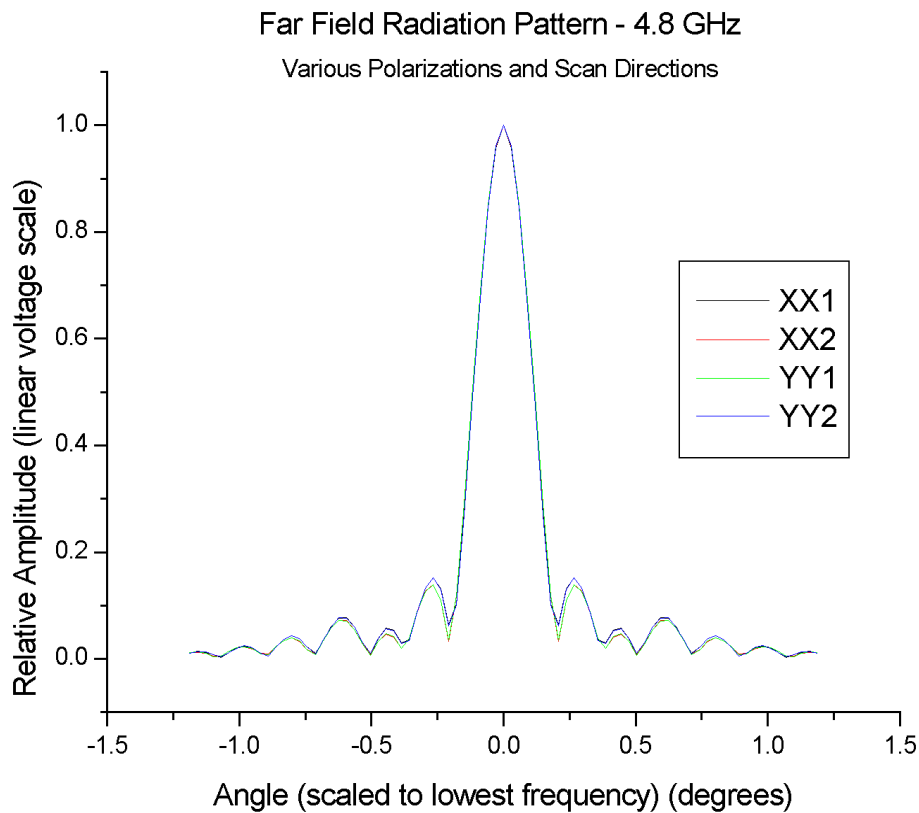

Figure 3 : Beam patterns for the two cross scans and in the XX and YY polarizations; all at 4.8 GHz.

The W band measurements showed asymmetry in the sidelobes between the polarisations and scan directions; see Figure 4.
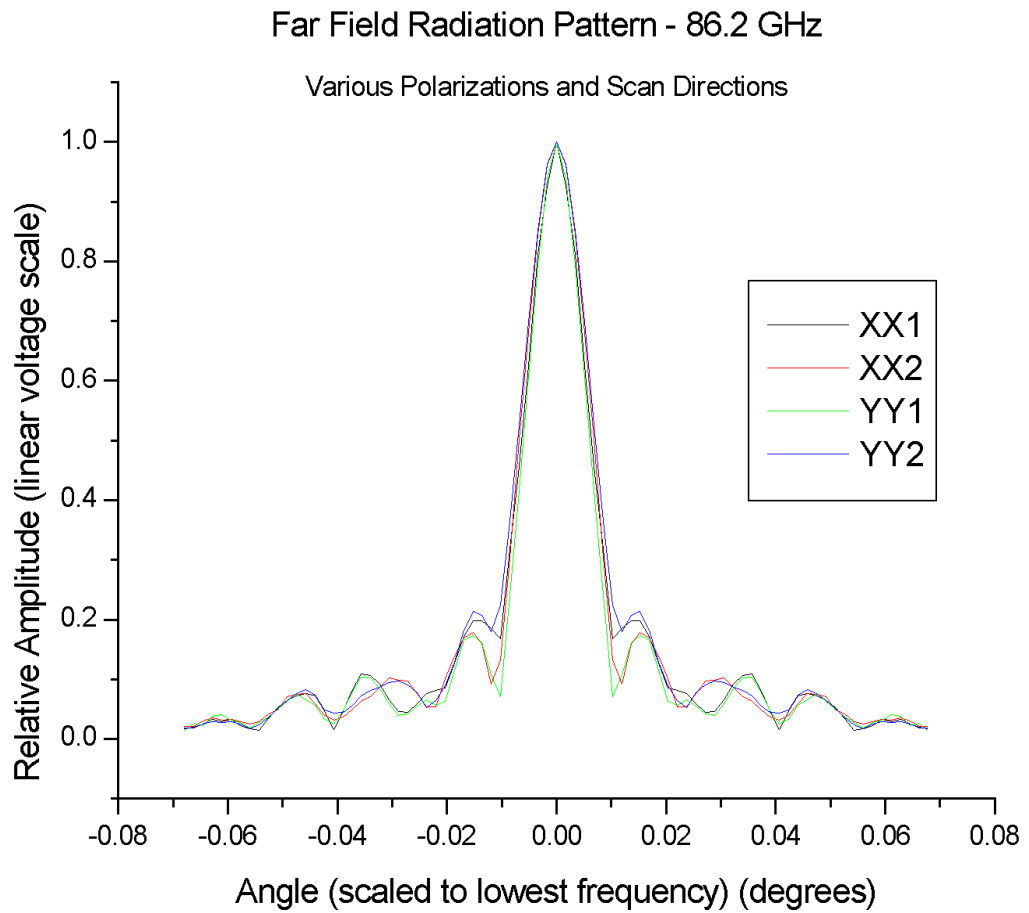

Figure 4 : Beam patterns for the two cross scans and in the XX and YY polarizations; all at 86.2 GHz.

As well as high-resolution scans, a series of large angle scans were taken at each of the measured frequencies. Shown (Figure 5) are the antenna field patterns measured out to large angles, averaged over each antenna, polarisation and scan direction.
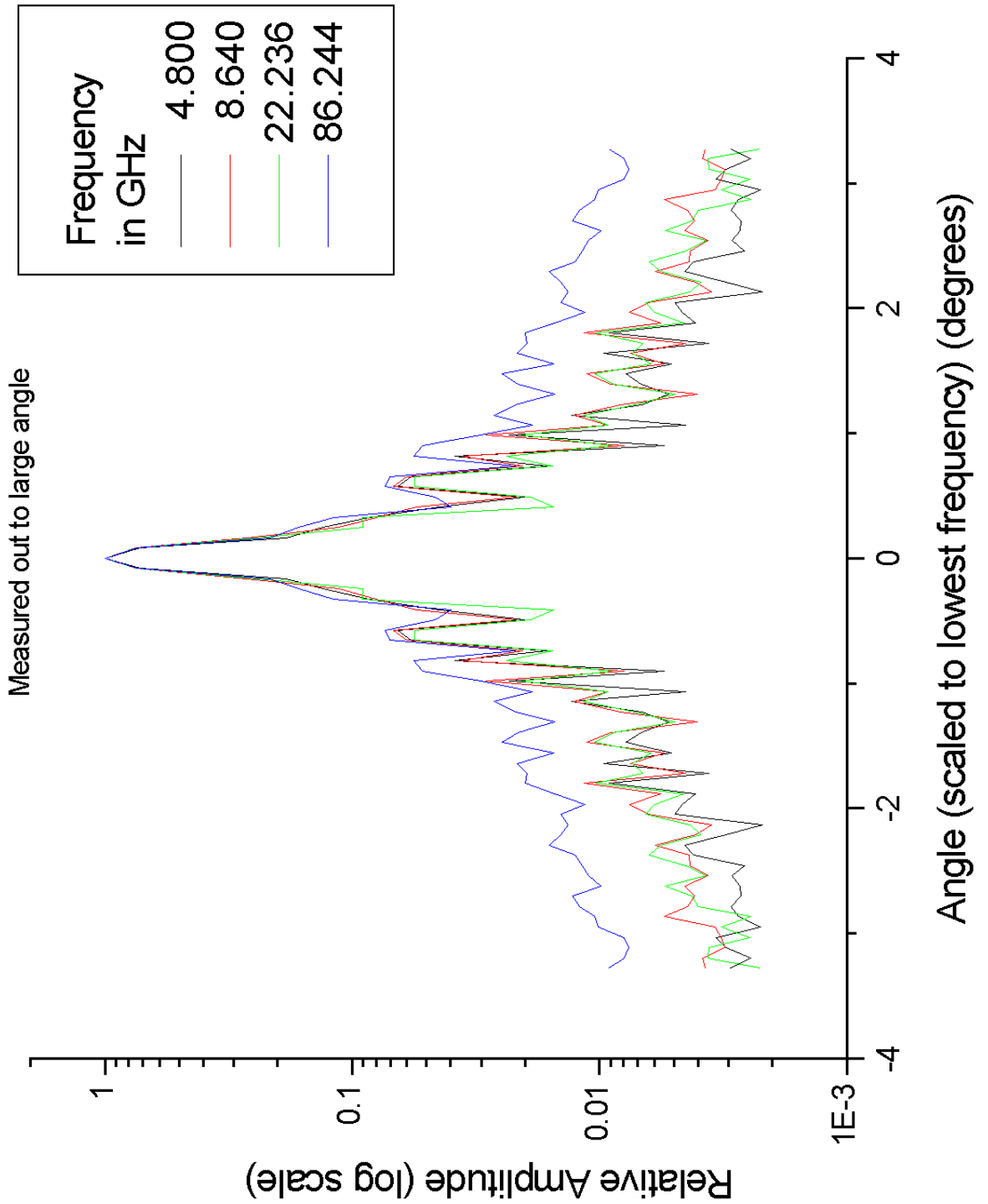
Figure 5 : Voltage Patterns out to large angles from the optical axis

Aperture Illumination

The aperture illumination for the telescope was then calculated using the Hankel transform, as discussed. The resulting aperture distributions are shown in Figure 6, for each of the measured frequencies. The aperture distributions computed from Hamming windowed scan data are shown in Figure 7. For each of these aperture distributions, the results have been normalised for unit area.

The resulting aperture distributions computed from the C, X & K band scans display sharp cut-offs at approximately 2 and 10.5 metres radii. These distances correspond closely with the edge of the vertex cone room (1.79 metres) and the edge of the dish (11 metres). The W band illumination shows a wider cut-off at the centre of the antenna (at about 2.5 metres).

The C, X and K band aperture distributions show, surprisingly, a decrement in illumination field amplitude between radii of 6.5 and 8 metres. We do not understand the cause for this reduction in aperture illumination over this radial distance. A number of causes have been hypothesised and investigated as possible causes, though none have as yet proven conclusive. Suggestions are welcome.

1. Because the decrement is seen over a limited range in radius, it is inferred that if the decrement is owing to an error in the scan data, the error is distributed over a wide range of offset angles. The error distribution over angles would have to scale with the frequency; which suggests that the error is in the mosaic positions file or in the reading of the file. We have looked at the sky coordinates of the scan data, in the visibility data file, and found that the offsets were as expected.

2. The decrement appears in the aperture illuminations computed using the scan data of single polarization products of individual baselines. If the decrement was due to the superposition of ringing effects from the inner and outer illumination edges, we would expect that the decrement ought to reduce with the Hamming window; however, the windowing did not lessen the trouble.

3. We independently analysed the visibility data, independently carried out the data calibration, separately wrote the routines for computing the aperture illumination and got identical results. Besides, the decrement is not obvious in the W band aperture illumination.

4. The Calibration in MIRIAD was investigated as a possible source of error by performing the transform on the same data without calibration, resulting in a similar overall behaviour.

5. The region of the decrement does not correspond to any particular ring of main reflector panels.

The C band illumination is fairly flat; the X-band illumination falls off at the edge to about 65 % of the field amplitude in the inner sectors of the aperture. This may be expected because in the CX feed, the feed beam pattern is narrower at X-band compared to that at C band frequencies. The mode converter design frequency for the

CX compact corrugated feed horn is 5.5 GHz, and f/f_i is 0.9 at 4.8 GHz; f/f_i is 1.6 at the X-band frequency of 8.6 GHz.

At 22.2 GHz, the aperture illumination falls off with increasing radius, again to about 65% of the value in the inner parts of the aperture.   The mode converter design frequency for the K-band horn is 17.91 GHz and f/f_i is 1.24 at the maser line frequency.

At 86 GHz, the decrease in aperture illumination with radius is relatively mild; the amplitude of the field at the edge falls to about 80% of the value in the inner parts. At this frequency, f/f_i is 1.06.
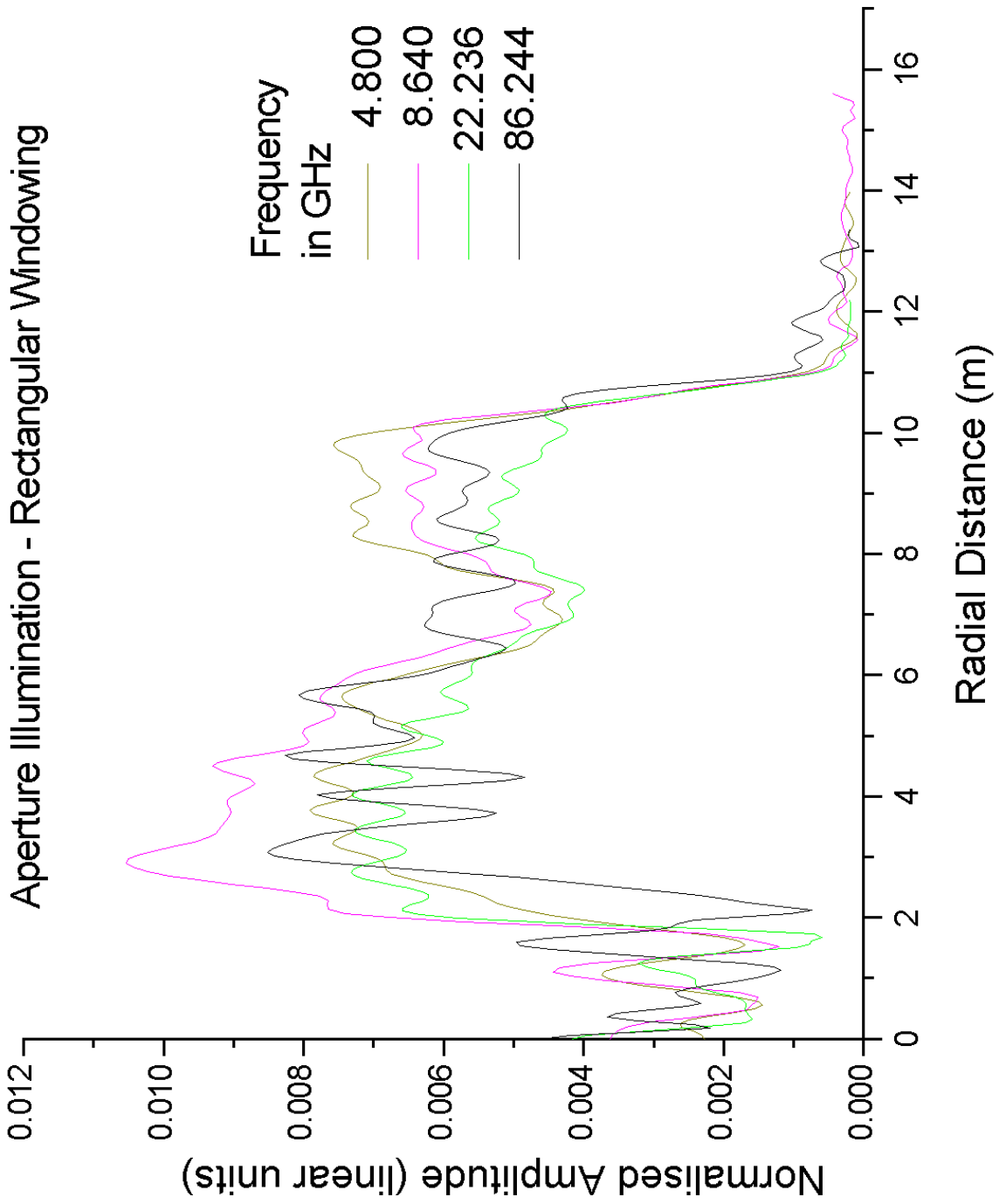
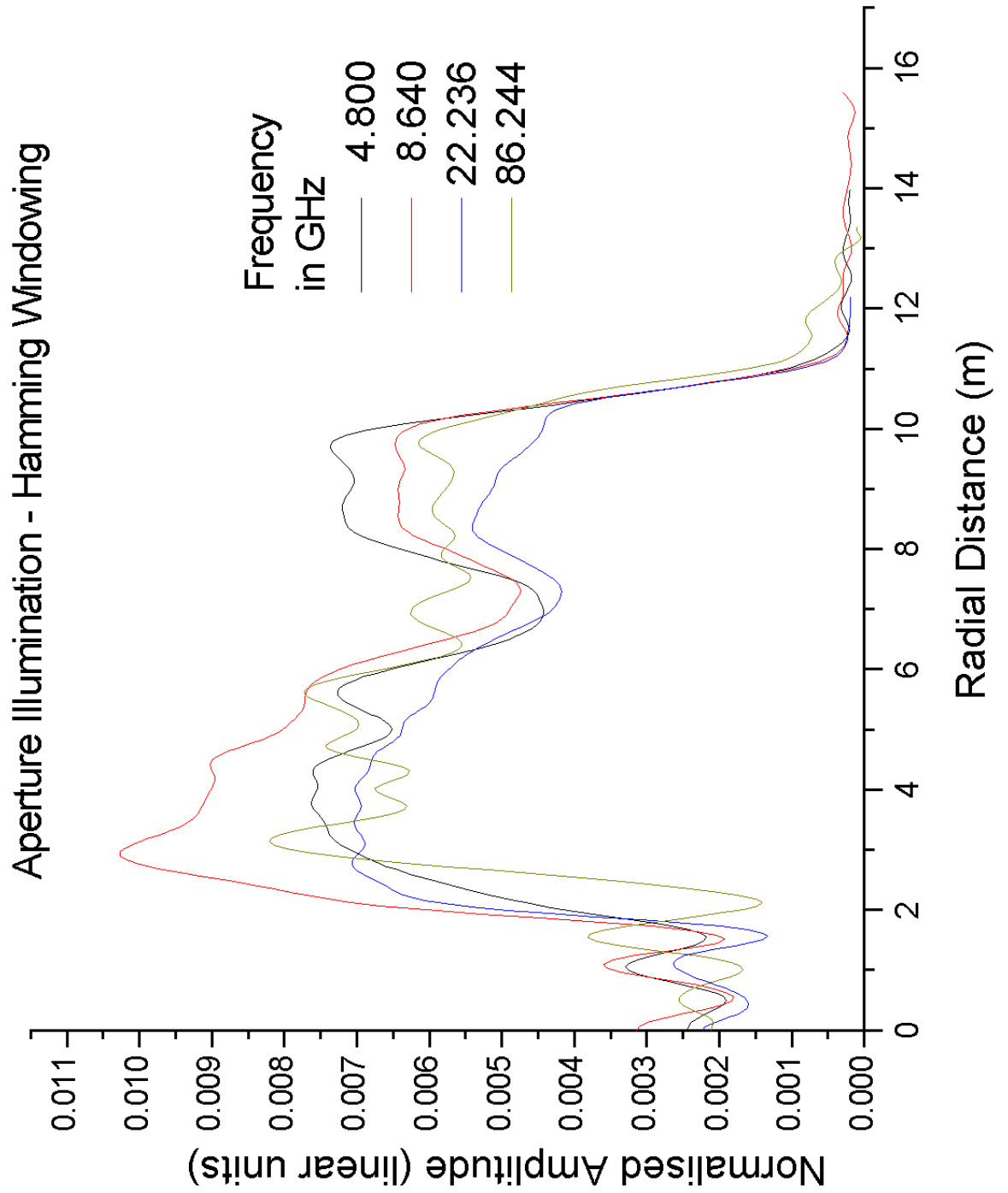**Figure 6 :** Aperture Distribution with Rectangular Windowing

Figure 7 : Aperture Distribution with Hamming Window

Appendix A.

Archived Data Location and Filenames.

This projects archival data is contain on a CD-ROM labelled **ATCA_20020703_C999**

The scans, naming convention and filenames are shown below.
Freq – refers to the frequency of the observations
Pass Number – refers to the pass number across the dish, where p1 and p2 refer to the large angle passes and c1 and c2 refer to the high resolution passes (small angle increments). Each mosaic point was given source names consecutively from 'p1' to 'p177' for the large angle and 'p1' to 'p81' for the small angle scans. The centre points are at 'p89' and 'p41' respectively and the calibration points are labelled 'c'. The two lower band measurements (C and X) each had two simultaneous frequency measurements, while the K and W band measurements were conducted using one frequency.

Raw Data Filenames

Freq (GHz)	Pass	Filename
4.8/4.928	P1	2002-07-03_1625.C999
4.8/4.928	P2	2002-07-03_1718.C999
4.8/4.928	C1	2002-07-03_1759.C999
4.8/4.928	C2	2002-07-03_1817.C999
8.64/8.512	P1	2002-07-03_1355.C999
8.64/8.512	P2	2002-07-03_1432.C999 2002-07-03_1518.C999*
8.64/8.512	C1	2002-07-03_1525.C999
8.64/8.512	C2	2002-07-03_1542.C999
22.2355	P1	2002-07-04_1026.C999
22.2355	P2	2002-07-04_1101.C999
22.2355	C1	2002-07-04_1136.C999
22.2355	C2	2002-07-04_1153.C999
86.2435	P1	2002-07-04_2125.C999
86.2435	P2	2002-07-04_2204.C999
86.2435	C1	2002-07-04_2045.C999
86.2435	C2	2002-07-04_2101.C999

*Restarted at p162 due to ACC failure between p156 and p177